Organic & Biomolecular Chemistry

Dynamic Article Links

Cite this: *Org. Biomol. Chem.*, 2012, **10**, 569

www.rsc.org/obc

PAPER

Impact of steric constraints on the product distribution of phosphate-branched oligonucleotide models of the large ribozymes†

Tuomas Lönnberg* and Kirsi-Maria Kero

Received 16th August 2011, Accepted 5th October 2011
DOI: 10.1039/c1ob06399e

To assess the extent to which steric constraints may influence the product distribution of the reactions of the large ribozymes, phosphate-branched oligonucleotides of varying length and sequence have been synthesized and their alkaline hydrolysis studied over a wide temperature range. At low temperatures, the branching trinucleoside-3′,3′,5′-monophosphate moiety is hydrolyzed almost exclusively by P–O3′ fission. At higher temperatures, P–O5′ fission competes, accounting at most for 22% of the overall reaction. The results suggest that steric constraints imposed by the secondary structure of the reaction site may significantly contribute to the observed regioselectivity of the transesterification reactions catalyzed by the large ribozymes.

Introduction

The transesterification reactions catalysed by the group I introns proceed *via* an acyclic pentacoordinated phosphorane resulting from the attack of a nucleoside 3′-oxygen on the phosphorus atom of an RNA phosphodiester linkage. This phosphorane is decomposed exclusively by fission of one of the P–O3′ bonds—no P–O5′ fission is detected (Scheme 1A).[1] The reactions of the other large ribozymes, the group II introns and the RNA subunit of RNase P, are characterized by similar regioselectivity.[2,3] On the other hand, cleavage of the P–O5′ bond accounts for 15% of the overall hydroxide ion catalyzed hydrolysis of the simple trinucleoside monophosphate model **1** (Scheme 1B), indicating that the P–O3′ bond is ruptured only 3 times as rapidly as the P–O5′ bond.[4] β_{lg} values of approximately –0.5 have been determined for the hydroxide ion catalyzed hydrolysis of both trialkyl[4] and dialkyl aryl[5] phosphates, indicating that the reaction is rather insensitive to the polar nature of the leaving group. The observed regioselectivity of the large ribozymes may, hence, not be explained simply in terms of different apicophilities and leaving-group properties of the 3′- and 5′-linked nucleosides. Another possibility would be that the neighboring 2′-OH group donates a hydrogen bond to the 3′-oxygen, making it a superior leaving group. While there is substantial evidence of hydrogen bond stabilization of the departing 3′-oxyanion by the vicinal 2′-OH function in the ribozyme reaction,[6] in related small molecular model systems some P–O5′ cleavage is still observed.[7,8] In line with these observations, theoretical studies on simple, unconstrained model compounds also suggest hydrogen bonding to a non-bridging phosphoryl oxygen rather than the departing 3′-oxygen.[9] It should be noted, however, that in the ribozyme structure the 2′-OH group flanking the scissile phosphodiester linkage is in all likelihood engaged in an extensive hydrogen bonding network that may well increase its acidity, as well as orient it favourably for interaction with the developing 3′-oxyanion.[9–12]

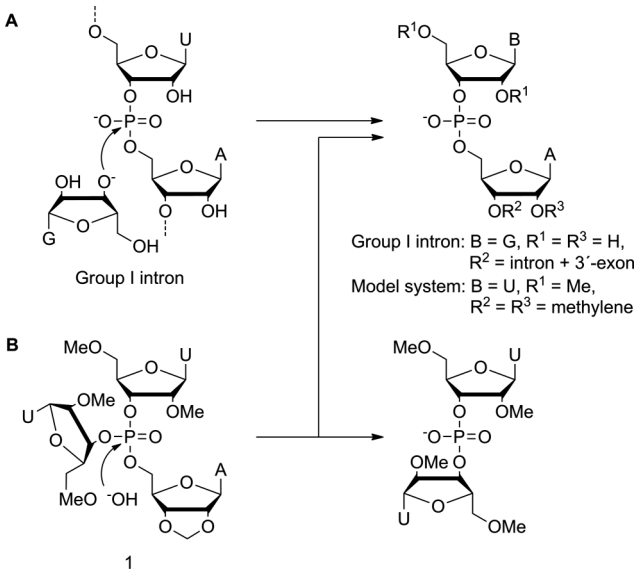

Scheme 1 Transesterification reactions of group I introns (A) proceed exclusively by cleavage of a P–O3′ bond, whereas in the hydrolysis of the trinucleoside-3′,3′,5′-monophosphates (B), cleavage of the P–O5′ bond competes.

Department of Chemistry, University of Turku, FIN-20014, Turku, Finland. E-mail: tuanlo@utu.fi; Fax: +358 2 333 6700; Tel: +358 2 333 6777

† Electronic supplementary information (ESI) available: ^{1}H, ^{13}C and ^{31}P NMR spectra of compound **4**, HPLC traces of the crude and mass spectra of the purified oligonucleotides **2a**, **2b** and **3**. See DOI: 10.1039/c1ob06399e

In the reactions of the group I introns, the scissile phosphodiester linkage is embedded within a double-helical region.[13,14] Hybridization makes RNA resistant to cleavage *via* intramolecular attack of the 2′-hydroxy function on phosphorus because base-stacking prevents the 5′-leaving group from assuming an apical position necessary for departure from the phosphorane intermediate.[15] To find out the extent to which steric constraints at the reaction site could also affect the product distribution of intermolecular reactions, such as the ones catalyzed by the large ribozymes, we have synthesized three branched 2′-OMe-RNA oligonucleotides containing a single trinucleoside phosphotriester linkage (Fig. 1). One of the oligonucleotides (**2a**) has the potential to form a hairpin loop, while another one (**2b**) is of the same length and base composition but its scrambled sequence is unlikely to form an ordered secondary structure. The third oligonucleotide (**3**) has otherwise the same sequence as **2a** but the self-complementary region composed of the ten 3′-terminal nucleotides has been deleted. Attack of a hydroxide ion on the phosphotriester linkage gives a phosphorane similar to that obtained by the attack of the 3′-hydroxy function of an external nucleoside on a 3′,5′-phosphodiester bond. According to Westheimer's rules, the two apical positions of the phosphorane will be occupied by the attacking hydroxide ion and one of the three nucleosides, with the remaining two nucleosides and the negatively charged non-bridging oxygen taking the three equatorial positions.[16] Depending on whether a 5′- or a 3′-linked nucleoside adopted an apical position in the initial step, the phosphorane species may decompose by cleavage of the P–O5′ or one of the P–O3′ bonds. Base-stacking of the oligonucleotide model, in particular the nucleosides flanking the phosphotriester linkage, is expected to impose additional constraints to the geometry of the phosphorane. If this is the case, then the product ratio (P–O5′ *vs.* P–O3′ fission) should change on varying the reaction temperature.

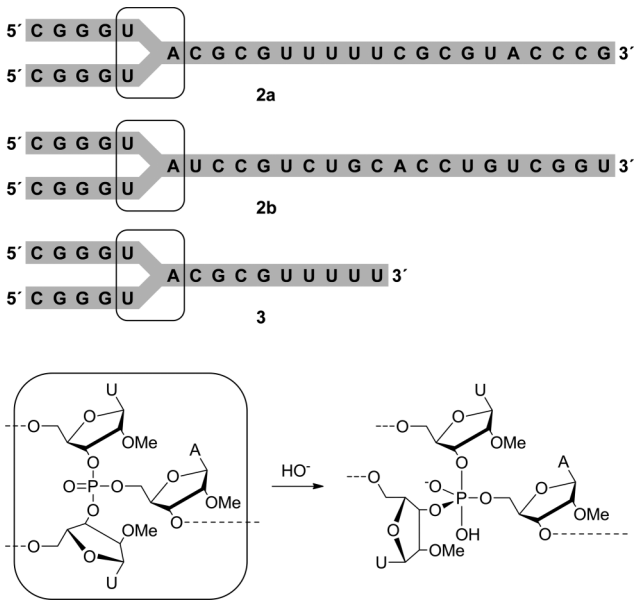

Fig. 1 Structures of the phosphate-branched oligonucleotide models **2a**, **2b** and **3** and attack of hydroxide ion on the phosphorus of the branching phosphotriester linkage.

Results and discussion

Synthesis of the oligonucleotide models

For branching the oligonucleotides at the desired phosphate, a dimeric bis[5′-*O*-(4,4′-dimethoxytrityl)-2′-*O*-methyluridin-3′-yl] *N*,*N*-diisopropylphosphoramidite building block (**4**) was first prepared by displacing both of the chloro substituents of *N*,*N*-diisopropylaminophosphorodichloridite with 5′-*O*-(4,4′-dimethoxytrityl)-2′-*O*-methyluridine (Scheme 2). The oligonucleotides were then assembled on a CPG-supported succinyl linker utilizing the standard phosphoramidite strategy for RNA (600 s coupling times). Coupling yield for the branching building block **4** was 55%; the other couplings proceeded with normal efficiency (*ca.* 99%). To avoid cleavage of the phosphotriester linkage, 40%

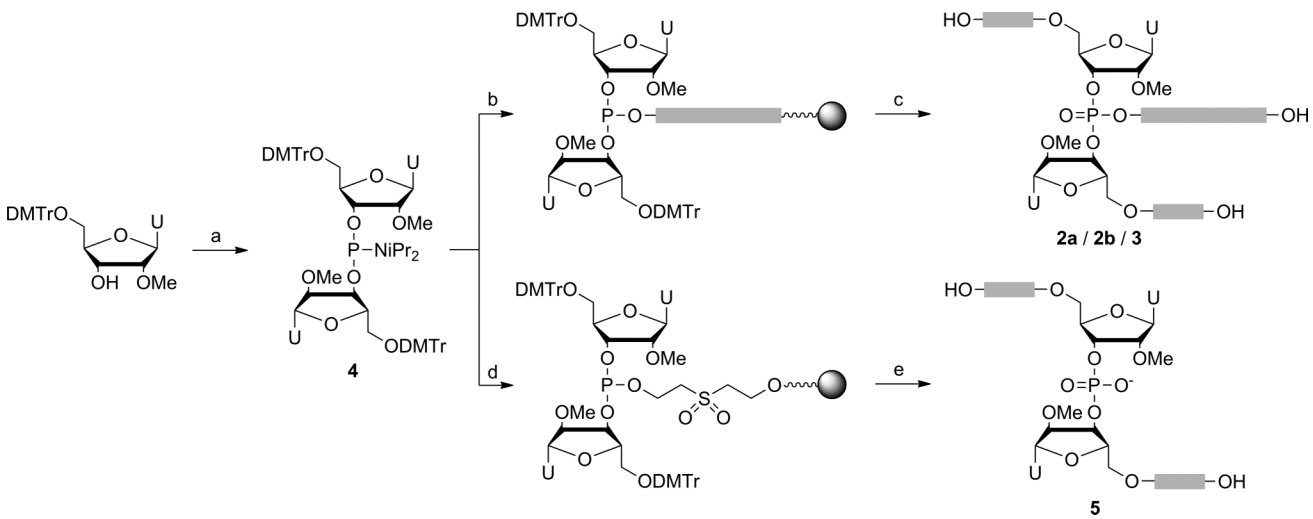

Scheme 2 Synthesis of the dimeric phosphoramidite building block **4**, the phosphate-branched oligonucleotides **2a**, **2b** and **3** and the 3′,3′-phosphodiester linkage containing oligonucleotide **5**. *Reagents and conditions*: (a) *N*,*N*-diisopropylaminophosphorodichloridite, Et_3N, CH_2Cl_2, (b) conventional phosphoramidite strategy on a succinyl linker, (c) 40% aq. $MeNH_2$, (d) conventional phosphoramidite strategy on a 2-(2-hydroxyethylsulfonyl)ethyl succinate linker, (e) 33% aq. NH_3.

aq. $MeNH_2$ (90 min at room temperature) was used instead of the conventional aq. NH_3 treatment for the deprotection and release of the oligonucleotides from the support. For a reference of one of the expected cleavage products, an oligonucleotide containing a 3′,3′ phosphodiester linkage (**5**) was synthesized on a CPG-supported 2-(2-hydroxyethylsulfonyl)ethyl succinate linker[17] (a universal linker designed for the synthesis of oligonucleotide-3′-monophosphates) using the dimeric phosphoramidite **4** as the first building block (Scheme 2). Coupling yield for the branching unit was 50%, after which elongation of both of the branches proceeded with normal efficiency. Conventional aq. NH_3 treatment was used for the deprotection and release of the oligonucleotide from the support. Finally, all of the oligonucleotide products were purified by RP HPLC. In the case of **2b**, additional purification by anion-exchange HPLC, followed by desalting by RP HPLC, was needed to obtain a pure sample.

Reaction pathways and product distribution

The hydroxide ion catalyzed hydrolysis of the oligonucleotide models was studied by anion-exchange HPLC at various NaOH concentrations over a temperature range of 3–90 °C. Two distinct sets of products were observed with all three models over the entire temperature range, one corresponding to P–O5′ (Route A) and another one to P–O3′ (Route B) fission (Scheme 3). Product distributions for the hydrolysis of the oligonucleotide models, as well as the trinucleoside monophosphate model **1**, were determined in 20 mmol L^{-1} aq. NaOH at various temperatures over a range of 3–90 °C by comparing the relative concentrations of oligonucleotide products **5** and **8** (or, in the case of **1**, 2′,3′-*O*-methyleneadenosine and 2′,5′-di-*O*-methyluridine) (Fig. 2). At 3 °C, cleavage of the P–O5′ bond accounts for 2.1, 2.6 and 4.1% of the overall hydrolysis of **2a**, **2b** and **3**, respectively. On going to higher temperatures, P–O5′ cleavage becomes more prominent, leveling off at approximately 22% for the long oligonucleotides **2a** and **2b** and approximately 18% for the short oligonucleotide **3**. In contrast, the product distribution of **1** is independent of temperature, P–O5′ fission accounting for approximately 16% of the overall reaction over the entire temperature range studied.

Table 1 Activation parameters for the hydroxide ion catalyzed hydrolysis of **1**, **2a**, **2b** and **3** in 20 mmol L^{-1} aq. NaOH; I(NaCl) = 0.10 M

Compound	$\Delta H^{\ddagger}$/kJ mol^{-1}	$\Delta S^{\ddagger}$/J K^{-1} mol^{-1}
1	56 ± 3	−140 ± 9
2a	45 ± 4	−200 ± 10
2b	41 ± 4	−210 ± 10
3	42 ± 4	−210 ± 10

Dependence of rate on pH and temperature

Between pH 10.3 and 11.3 (in 2–20 mmol L^{-1} NaOH), the hydrolysis of **3** is first order in [HO^-] and approximately 6-fold slower than previously observed for **1** (Fig. 3). The rates of hydrolysis of **2a** and **2b** were essentially identical to that of **3** (data not shown). The rate constants determined at various temperatures allow calculation of activation parameters for the hydroxide ion catalysed hydrolysis of **1**, **2a**, **2b** and **3** using the Eyring equation (Fig. 4). The values obtained are summarized in Table 1. In all cases, the entropy of activation is clearly negative, consistent with the associative mechanism proposed for the alkaline hydrolysis of phosphotriesters.[18]

Conformation of the oligonucleotide models

To quantify the thermal weakening of the base-stacking of the oligonucleotide models, their CD spectra were measured at 3 or 4 °C intervals over a range of 3–90 °C in 20 mmol L^{-1} aq. NaOH (Fig. 5). In all cases, the spectra were characteristic of single-stranded RNA (A-type helix)[19] and gradual loss of ellipticity was observed on increasing temperature. Plots of the relative decrease in ΔA at 273 nm as a function of temperature are presented in Fig. 2, overlaid with the observed product distributions.

At the low and high ends of the temperature range, *i.e.* below 30 °C and above 70 °C, the product distributions (ratio of P–O5′

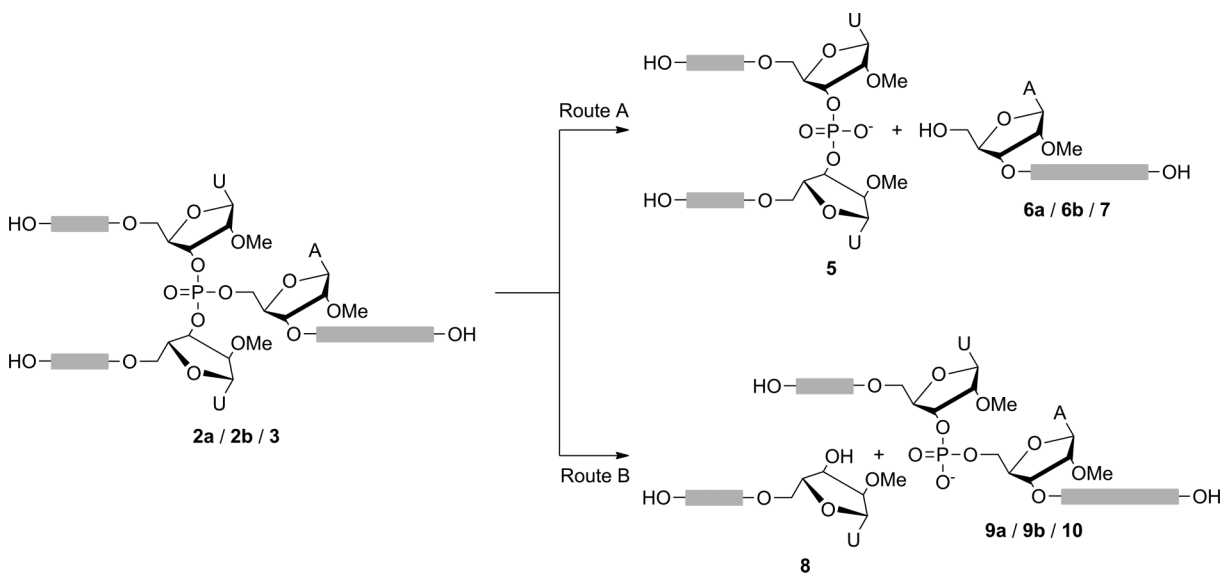

Scheme 3 Hydrolytic reaction pathways of the phosphate-branched oligonucleotides **2a**, **2b** and **3**.

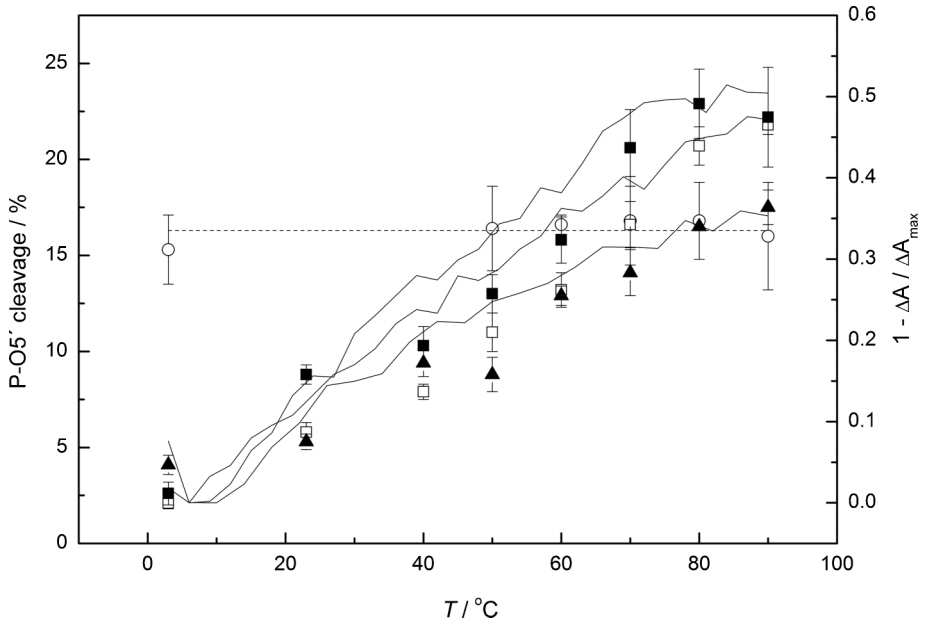

Fig. 2 The contribution of P–O5′ cleavage to the overall hydrolysis of the trinucleoside monophosphate **1** (○) and the phosphate-branched oligonucleotides **2a** (□), **2b** (■) and **3** (▲) as a function of temperature in 20 mmol L^{-1} aq. NaOH; I = 0.10 mol L^{-1}. The solid lines represent the observed thermal loss of ellipticity for the oligonucleotide models and the dashed line the average ratio of P–O5′ cleavage to the overall hydrolysis of **1** (16.3%).

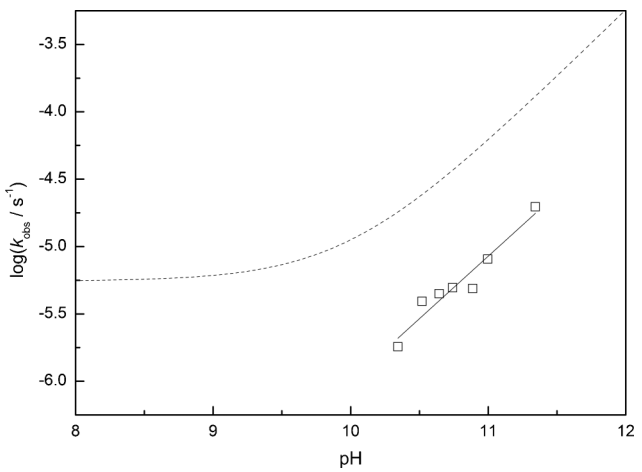

Fig. 3 pH–rate profile for the overall hydrolysis of the phosphate-branched oligonucleotide **3** (□) and the trinucleoside monophosphate **1** (dashed line) at 50 °C.

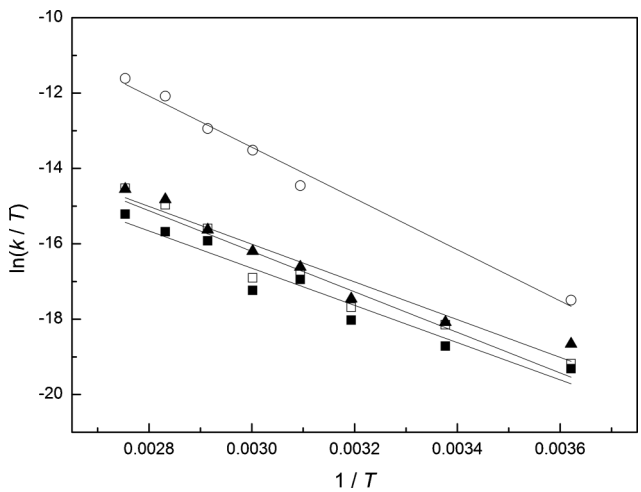

Fig. 4 Eyring plots for the hydroxide ion catalyzed hydrolysis of **1**, **2a**, **2b** and **3** in 20 mmol L^{-1} aq. NaOH; I(NaCl) = 0.10 M.

fission to the overall reaction) correlate reasonably well with the loss of ellipticity (Fig. 2). At intermediate temperatures, on the other hand, the points for the product distributions systematically fall under the lines for the loss of ellipticity. It should be borne in mind, however, that the CD spectra reflect changes in the global structure of the oligonucleotides, whereas the course of the reactions of the phosphotriester linkage are in all likelihood largely dictated by the local structure around this branching site.

The UV spectra of the oligonucleotide models, measured over a temperature range of 3–90 °C in 20 mM aq. NaOH, show an increase in absorbance of only approximately 5% in each case (data not shown). In other words, despite its self-complementary sequence, **2a** does not exhibit an increase in absorbance typical for thermal denaturation of a double-stranded oligonucleotide. In the light of previous studies, in the highly alkaline reaction solutions (pH = 11.3 at 50 °C) used, hybridization of **2a** into a hairpin structure seems rather unlikely.[20,21] Instead, the temperature-dependent product mixture probably reflects weakening of base-stacking at high temperatures (Fig. 6). The longer stacks of **2a** and **2b** may be more highly ordered than the relatively short stack of **3**, resulting in the greater observed temperature dependence. Curiously, while with the short model **3** the extent of P–O5′ cleavage seems to plateau on the level observed for the trinucleoside monophosphate model **1** over the entire temperature range studied (*ca.* 17%), the longer models **2a** and **2b** exhibit somewhat higher ratios of P–O5′ fission to overall reaction (*ca.* 22%).

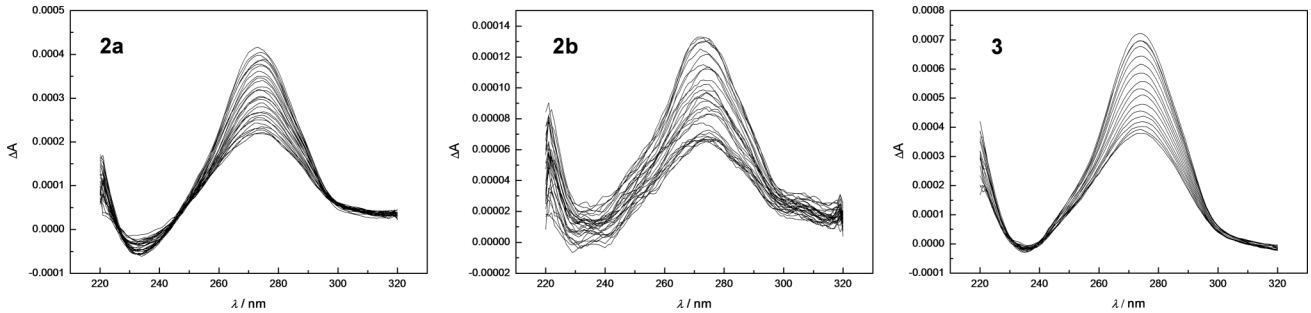

Fig. 5 CD spectra of **2a**, **2b** and **3** as a function of temperature.

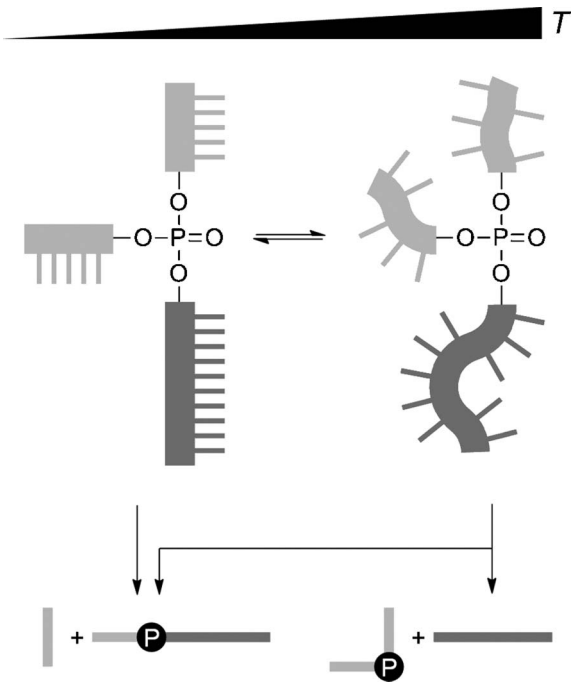

Fig. 6 Thermal disruption of the base-stacking of the oligonucleotide model and the resulting loss of regioselectivity of the hydrolysis of the branching phosphotriester linkage.

Under conditions where the nucleobases exist in the nonionized form, *i.e.* between pH 4 and 9, the hydrolysis of the trinucleoside 3′,3′,5′-monophosphate model **1** proceeds predominantly by a pH-independent elimination and attack of hydroxide ion on the phosphorus is observed only at pH > 10.[4] In other words, the alkaline conditions needed for the hydroxide ion catalyzed reaction to be detected preclude studying the reactions of a phosphotriester linkage within a double-stranded oligonucleotide by the present method. It seems likely, however, that hybridization of the substrate oligonucleotide would inhibit the cleavage of the P–O5′ bond even further.

Conclusions

The present results indicate that base-stacking of an oligonucleotide markedly retards cleavage of the P–O5′ bond even when the reaction is initiated by attack of a sterically unhindered external nucleophile (a hydroxide ion) on the phosphorus. The reactions catalysed by the large ribozymes proceed by attack of a nucleoside 3′- (or 2′-) oxygen and much more rapidly than the model reactions but the factors affecting the course of the step determining the product distribution, *viz.* P–O bond fission, may be expected to be the same. While the reaction conditions used in this study are too alkaline for hybridization of the oligonucleotides, the ribozymes work under physiological conditions and recognition of the reactive site by Watson–Crick base-pairing seems to be a common strategy.[13,14,22] In other words, in the reactions catalysed by the large ribozymes the reactive phosphodiester linkage is typically embedded in a double-helical stem which, in all likelihood, has an effect on the product distribution that is similar to but greater than the one reported in this paper. Accordingly, the observed regioselectivity of the large ribozymes may largely be explained by steric constraints imposed by the highly ordered environment of the catalytic centre.

Experimental section

General

5′-*O*-(4,4′-Dimethoxytrityl)-2′-*O*-methyluridine was prepared from 2′-*O*-methyluridine by conventional methods. 2′-*O*-Methyluridine and *N*,*N*-diisopropylaminophosphorodichloridite were commercial products that were used as received. For the triethylammonium acetate buffer used in HPLC chromatography, triethylamine was distilled before using. The NMR spectra were recorded with a Bruker Avance 500 NMR spectrometer, the mass spectra with a MicroTOF Q high resolution ESI mass spectrometer and the CD spectra with an Applied Photophysics Chirascan spectropolarimeter. The oligonucleotides were assembled on an Applied Biosystems 392 or 3400 DNA synthesizer.

Kinetic measurements

Hydrolytic reactions of the phosphate-branched oligonucleotide models **2a**, **2b** and **3** were carried out in sealed tubes immersed in a water bath, the temperature of which was controlled within ±0.1 °C (the temperature range used was 3–90 °C). The hydroxide ion concentration of the solutions was adjusted to 1–20 mmol L^{-1} with NaOH and the ionic strength to 0.10 mol L^{-1} with NaCl. The initial concentration of the starting material was approximately 1 μmol L^{-1}. The compositions of the samples withdrawn at appropriate time intervals were analyzed by anion-exchange HPLC on a Dionex DNASwift™ SAX-1S column (5 × 150 mm, monolithic) thermostated to 60 °C eluting with a linear gradient of 0.33 mol L^{-1} $NaClO_4$ (10 → 60% in 16 min, flow rate = 1.5 mL min^{-1}) in

20 mmol L^{-1} TRIS buffer (pH = 7.0). The observed retention times (t_R/min) for the hydrolytic products of **2a**, **2b** and **3** were as follows: 4.4 (**8**), 8.6 (**7**), 9.1 (**5**), 10.5 (**10**), 10.9 (**6a**), 11.4 (**6b**), 11.9 (**9a**), 12.4 (**9b**), 12.7 (**2b**), 12.9 (**2a**), 14.6 (**3**). The products were characterized by spiking with authentic samples. For determining the product ratios of the reactions, the peak areas of **8** and **5** were converted to relative concentrations by using molar absorption coefficients calculated by an implementation of the nearest-neighbors method. Oligonucleotides **8** and **5** are the two hydrolysis products common to all of the models used and the two 5′→3′ arms of **5** have the same sequence as **8**, ensuring reliable comparison.

Synthesis of the branched oligonucleotides (2a, 2b and 3)

The oligonucleotides were assembled on a CPG-supported succinyl linker at a loading of 27 μmol g^{-1}. Standard phosphoramidite strategy for RNA (600 s coupling time) was used throughout the sequences. Based on trityl response, coupling yield for the dimeric branching phosphoramidite **4** was 55% with both **2** and **3** and the other couplings proceeding with normal efficiency. To avoid hydrolytic cleavage of the phosphotriester linkage, 40% aq. $MeNH_2$ (90 min at room temperature) was used instead of the conventional aq. ammonia treatment for the deprotection and release of the oligonucleotides from the support. The released products were purified by RP HPLC on a Thermo ODS Hypersil column (250 × 4.6 mm, 5 μm) eluting with a mixture of 0.10 mol L^{-1} triethylammonium acetate and MeCN. HPLC traces of the crude product mixtures are presented in the ESI. HRMS (ESI^-): *m/z* calcd 1417.3941 (**2a** and **2b**)/940.7388 (**3**) obsd 1417.5095 (**2a**)/1417.7042 (**2b**)/940.7260 (**3**) $[M - 7H]^{7-}$.

Synthesis of the 3′,3′-phosphodiester linkage containing oligonucleotide (5)

The oligonucleotide was assembled on a CPG-supported 2-(2-hydroxyethylsulfonyl)ethyl-2-succinyl linker[17] at a loading of 38 μmol g^{-1} using the dimeric phosphoramidite **4** as the first building block. The standard phosphoramidite strategy for RNA (600 s coupling time) was used throughout the sequence. Coupling yield for the branching unit was 50%, after which elongation of both of the branches proceeded with normal efficiency. Conventional aq. NH_3 treatment was used for the deprotection and release of the oligonucleotide from the support. The released product was purified by RP HPLC on a Thermo ODS Hypersil column (250 × 4.6 mm, 5 μm) eluting with a mixture of 0.10 mol L^{-1} triethylammonium acetate and MeCN. HRMS (ESI^-): *m/z* calcd 1122.8740 obsd 1122.8567 $[M - 3H]^{3-}$.

Bis[5′-*O*-(4,4′-dimethoxytrityl)-2′-*O*-methyluridin-3′-yl] *N*,*N*-diisopropylphosphoramidite (4)

5′-*O*-(4,4′-Dimethoxytrityl)-2′-*O*-methyluridine (1.0033 g, 1.79 mmol) was coevaporated three times from anhydrous pyridine. The residue was dissolved in CH_2Cl_2 (2.0 mL), triethylamine (1.37 mL, 9.83 mmol) and *N*,*N*-diisopropylaminophosphorodichloridite (0.150 mL, 0.81 mmol) were added and the resulting mixture was stirred for 5 h at room temperature. Saturated aq. $NaHCO_3$ (80 mL) was added and the mixture was extracted with ethyl acetate. The organic phase was dried with Na_2SO_4 and evaporated to dryness and the residue was purified on a silica gel column eluting with a mixture of triethylamine, hexane and ethyl acetate (1 : 10 : 89, v/v). Yield 0.1667 g (7%). ^1H NMR (d_H)(500 MHz, MeCN-d_3): 9.51 (s, 2H), 7.78 (d, 1H, J = 8.2 Hz), 7.64 (d, 1H, J = 8.2 Hz), 7.45 (m, 2H), 7.41 (m, 2H), 7.36–7.24 (m, 14H), 6.86 (m, 8H), 5.95 (d, 1H, J = 3.7 Hz), 5.91 (d, 1H, J = 3.8 Hz), 5.37 (d, 1H, J = 8.2 Hz), 5.30 (d, 1H, J = 8.1 Hz), 4.66 (ddd, 1H, $J_1 = J_2$ = 5.6 Hz, J_3 = 9.2 Hz), 4.27 (ddd, 1H, $J_1 = J_2$ = 5.6 Hz, J_3 = 9.2 Hz), 4.19 (ddd, 1H, $J_1 = J_2$ = 2.8 Hz, J_3 = 5.8 Hz), 4.00 (m, 3H), 3.77 (s, 6H), 3.74 (s, 3H), 3.73 (s, 3H), 3.58–3.49 (m, 2H), 3.51 (s, 3H), 3.44–3.36 (m, 3H), 3.41 (s, 3H), 3.30 (dd, 1H, J_1 = 4.2 Hz, J_2 = 10.9 Hz), 1.14 (d, 6H, J = 6.8 Hz), 1.05 (d, 6H, J = 6.8 Hz). ^{31}P NMR (d_P)(202 MHz, MeCN-d_3): 148.6 (s, 1P). HRMS (ESI^+): *m/z* calcd 1250.5097 obsd 1250.5029 $[M + H]^+$.

Acknowledgements

Financial support from the Academy of Finland is gratefully recognized.

Notes and references

1 A. J. Zaug, P. J. Grabowski and T. R. Cech, *Nature*, 1983, **301**, 578.
2 D. L. Daniels, W. J. Michels and A. M. Pyle, *J. Mol. Biol.*, 1996, **256**, 31.
3 K. Haydock and L. C. Allen, *Prog. Clin. Biol. Res.*, 1985, **172A**, 87.
4 T. Lönnberg and S. Mikkola, *J. Org. Chem.*, 2004, **69**, 802.
5 S. A. Khan and A. J. Kirby, *J. Chem. Soc. B*, 1970, 1172; R. Rowell and D. G. Gorenstein, *J. Am. Chem. Soc.*, 1981, **103**, 5894; S.-B. Hong and F. M. Rauschel, *Biochemistry*, 1996, **35**, 10904.
6 A. Yoshida, S. Shan, D. Herschlag and J. A. Piccirilli, *Chem. Biol.*, 2000, **7**, 85.
7 T. Lönnberg and J. Korhonen, *J. Am. Chem. Soc.*, 2005, **127**, 7752.
8 T. Lönnberg, M. Ora, S. Virtanen and H. Lönnberg, *Chem.–Eur. J.*, 2007, **13**, 4614.
9 S. Bakalova, W. Siebrand, A. Fernandez-Ramos, Z. Smedarchina and D. D. Petkov, *J. Phys. Chem. B*, 2002, **106**, 1476.
10 M. Forconi, R. N. Sengupta, J. A. Piccirilli and D. Herschlag, *Biochemistry*, 2010, **49**, 2753.
11 J. L. Hougland, R. N. Sengupta, Q. Dai, S. K. Deb and J. A. Piccirilli, *Biochemistry*, 2008, **47**, 7684.
12 S. A. Strobel and L. Ortoleva-Donnelly, *Chem. Biol.*, 1999, **6**, 153.
13 M. D. Been and T. R. Cech, *Cell*, 1987, **50**, 951.
14 Q. Vicens and T. R. Cech, *Trends Biochem. Sci.*, 2006, **31**, 41.
15 D. A. Usher and A. H. McHale, *Proc. Natl. Acad. Sci. U. S. A.*, 1976, **73**, 1149.
16 F. H. Westheimer, *Acc. Chem. Res.*, 1968, **1**, 70.
17 T. Horn and M. Urdea, *Tetrahedron Lett.*, 1986, **27**, 4705.
18 P. W. C. Barnard, C. A. Bunton, D. R. Llewellyn, C. A. Vernon and V. A. Welch, *J. Chem. Soc.*, 1961, 2670; E. M. Thain, *J. Chem. Soc.*, 1957, 4694.
19 J. Brahms, A. M. Michelson and K. E. Holde, *J. Mol. Biol.*, 1966, **15**, 467; J. Brahms, J. C. Maurizot and A. M. Michelson, *J. Mol. Biol.*, 1967, **25**, 465; C. A. Busch and H. A. Scheraga, *Biopolymers*, 1969, **7**, 395; H. T. Steely, Jr., D. M. Gray and R. L. Ratliff, *Nucleic Acids Res.*, 1986, **14**, 10071.
20 D. M. Crothers, *J. Mol. Biol.*, 1964, **9**, 712.
21 F. W. Studier, *J. Mol. Biol.*, 1965, **11**, 373.
22 T. Lönnberg, *Chem.–Eur. J.*, 2011, **17**, 7140.

